



# Characterization of fouled ultrafiltration membranes from a full-scale wastewater reclamation plant in iron and steel industry

P.-H. Lin<sup>1</sup> · Y.-C. Su<sup>2</sup> · C.-L. Chen<sup>3,4</sup> · I.-Y. Tsao<sup>5</sup>

Received: 26 August 2022 / Revised: 21 December 2022 / Accepted: 30 December 2022 / Published online: 7 January 2023

© The Author(s) under exclusive licence to Iranian Society of Environmentalists (IRSEN) and Science and Research Branch, Islamic Azad University 2023

## Abstract

Iron- and steel-making industry is one of the most water-intensive industries. An industrial wastewater purification plant using ultrafiltration and reverse osmosis is utilized by the iron and steel production industry to reclaim wastewater from the manufacturing processes. After sustained operation, the ultrafiltration membranes suffered from severe fouling problems. The frequent and necessary chemical cleaning results in raised operating cost, reduced permeate, and shortened membrane lifetime. The objective of this research was to identify the major foulants that result from long-term real-world operation of the ultrafiltration system. The fouled ultrafiltration membrane samples were collected four times during a 1.5-year period. Scanning electron microscope with energy-dispersive spectrometer, loss on ignition, and fouling resistance analysis were conducted to characterize the foulants. We identify iron (Fe) and manganese (Mn) oxides as the major foulants on the membrane surface and in the pores. We also demonstrate that irrecoverable fouling as the major contributor to fouling resistance, accounting for approximately 43~47% of the total increase in resistance. Based on our data, the irrecoverable fouling likely begins with the deposit of Fe and Mn ions and oxide particulates within the membrane pores, following by accumulation of additional oxides in part through an autocatalytic process, which ultimately leads to pore clogging. Therefore, pretreatment of the ultrafiltration influent to remove Fe and Mn ions can be a sound strategy to mitigate irrecoverable fouling.

**Keywords** Iron oxide · Manganese oxide · Membrane fouling · Ultrafiltration · Wastewater reclamation

---

Editorial responsibility: Lifeng Yin.

✉ P.-H. Lin  
phlin@ncu.edu.tw

<sup>1</sup> Graduate Institute of Environmental Engineering, National Central University, No. 300, Zhongda Rd., Zhongli District, Taoyuan City 32001, Taiwan

<sup>2</sup> New Materials Research and Development Department, China Steel Corporation, Hsiao Kang, Kaohsiung 81233, Taiwan

<sup>3</sup> Department of Safety, Health and Environmental Engineering, Ming Chi University of Technology, No. 84 Gungjuan Rd., Taishan Dist., New Taipei City 24301, Taiwan

<sup>4</sup> Center for Environmental Sustainability and Human Health, Ming Chi University of Technology, No. 84 Gungjuan Rd., Taishan Dist., New Taipei City 24301, Taiwan

<sup>5</sup> Institute of Materials Science and Engineering, National Central University, No. 300, Zhongda Rd., Zhongli District, Taoyuan City 32001, Taiwan

## Introduction

Iron- and steel-making industry is one of the most water-intensive and energy-intensive industries. Considerable quantities of water are mainly consumed for production departments, cooling systems, coke ovens, particularly in the integrated route, which produces steel from iron ore and fossils (Colla et al. 2016). Wastewaters generated from various manufacture processes have specific characteristics and generally require further treatment for reuse due to the poor quality of the water. For water resource conservation, the iron and steel industries around the world are focusing on the rationalization of water resources to minimize the water consumption per ton of steel (Hird 2006; Huang et al. 2011). Thus, the development of suitable treatment processes to reclaim wastewater is a crucial step to increase the water recycling rate, thereby decreasing overall water consumption.

Ultrafiltration (UF) is one of the most promising processes for the treatment of wastewater in industrial sectors. It is commonly deployed as a pretreatment process for



reverse osmosis (RO) when water reclamation is desired. UF can efficiently remove high molecular weight organic matters, large colloids, and suspended particles from wastewater. As a result, the suspended solids and oxygen demand can be effectively reduced (Michael-Kordatou et al. 2015; Mohammadi and Esmaeilifar 2004; Petrinic et al. 2015; Racar et al. 2017). In addition, the application of UF allows several industries to become more environmentally friendly by decreasing waste production and by increasing the reuse of high-value components (Al Aani et al. 2018; Rohani et al. 2011). However, membrane fouling has emerged as a serious obstacle that limits the application of UF. Membrane fouling leads to decreased permeate flux, shortened longevity of the membrane modules, and decreased efficiency, which in turn increases energy consumption. Membrane cleaning, although can partially control membrane fouling, requires increased chemical usage and additional labor for maintenance. Therefore, membrane fouling not only decreases the efficacy but also increases the cost of operation of UF (Jafari et al. 2021; Porcelli and Judd 2010).

Membrane fouling occurs as the substances in the influent leave the liquid phase to form a layer on either the membrane surface (i.e., external fouling) or inside the membrane pores (i.e., internal fouling) (D'Souza and Mawson 2005). It could lead to irreversible loss of the permeability of a membrane. Mechanisms involved in membrane fouling commonly include adsorption, pore blocking, and cake or gel formation (Gao et al. 2011; Guo et al. 2012; Katsoufidou et al. 2010). Adsorption takes place when colloids/solutes and the membrane interact through electrostatic attraction, van der Waals forces, or chemical bonding, is a process of thermodynamic equilibrium (Shi et al. 2014). Pore blocking refers to the entire or partial blockage of membrane pores by particles and colloids (Field and Wu 2011). Cake formation takes places when colloids precipitate layer by layer on the membrane surface, resulting in an additional resistance to the membrane flux (Shi et al. 2014). Gel formation occurs when extremely concentrated macromolecules have accumulated and consolidated in the immediate vicinity of the membrane surface through concentration polarization (Baker 2004; Bourgeois et al. 2001; Shi 2014).

Numerous methods have been devised to control and prevent UF membrane fouling, such as pretreatment of the influent by oxidation, coagulation and/or flocculation, disinfection, acidification, media filtration, and chemical modification (Colla Branca Rosito Lucca Vivas and Delmiro 2016; Shi 2014). Periodic membrane backwash and cleaning can significantly recover the permeate flux by removing foulants on the membrane surface (Nguyen and Roddick 2011). Optimization of membrane cleaning processes requires a comprehensive understanding of complex interactions between the foulants and membranes (Shi et al. 2014). The effectiveness of a method will be evaluated based on several factors,

including chemical costs, sanitation costs, treatment efficacy, impact on membrane life, etc. To understand the mechanism of membrane fouling, knowing how the composition of the treated wastewater (metals, colloids, microorganisms, etc.) interacts with the UF membrane will allow the development of appropriate control and cleaning methods. In the study conducted by Lee et al., they applied back-washable micro-filtration (BMF) and RO to treat the effluent from secondary treatment for water recycle in a steel company (Lee et al. 2005). However, membrane fouling in the MF system was not discussed in this study. In another study using a pilot-scale UF/RO system to reclaim the wastewater from a steel manufacturing industry, Choi et al. demonstrated that algae and bacteria are the predominant foulants (Choi et al. 2015). However, the study was only conducted within a relatively short period of time (16 days), but a UF membrane system for water reclamation typically lasts years. How membrane fouling occurs in the long term remains poorly understood. Therefore, long-term field investigations will be essential in uncovering the mechanism of membrane fouling in the UF treatment of iron- and steel-making wastewater. These investigation will provide the basis for improvement or novel formulation of pretreatment and cleaning protocols (Darton et al. 2004).

In this study, wastewater produced from an integrated steelwork in Taiwan was treated and reclaimed by their own industrial wastewater purification plant (IWPP). The treatment process includes coagulation, flocculation, sedimentation, fiber filtration, UF, RO, and ion exchange (IX). However, after 3 years of operation, the UF membranes were severely fouled. The trans-membrane pressure (TMP) often achieved the threshold pressure ( $-45$  Kpa) within 2–3 days, while the new membrane can run without clean-in-place (CIP) for approximately 30 days. As a result of fouling, the permeate flux was dramatically decreased and the operating cost was significantly increased. Therefore, the objective of this research is to identify the major foulants that clogged the UF system in the IWPP. To the best of authors' knowledge, this is the first research to investigate the foulants and the fouling mechanisms of the UF membranes in the setting of iron and steel manufacturing wastewater treatment in a full-scale operating reclamation plant. The membranes from the UF cassettes were sampled serially four times during a 1.5-year period. To identify and characterize foulants, we studied the sampled membranes with scanning electron microscopy with energy-dispersive spectrometer (SEM/EDS). Loss-on-ignition (LOI) analysis allows us to further characterize the organic and inorganic components of the foulants. Lastly, we apply resistance-in-series (RIS) models to determine various responsible fouling resistances of the fouled membranes in a single-membrane reactor. All experiments were conducted in Taiwan during the years of 2019 and 2020.



## Materials and methods

### IWPP treatment process

The schematic diagram of the IWPP treatment processes is shown in Fig. 1. The influent wastewater streams of the IWPP were mixtures of blast furnace gas scrubbing wastewater, cold rolling wastewater, and direct and indirect cooling water. The wastewater streams were initially treated with coagulation, flocculation, sedimentation, and fiber filtration. The resultant filtrate was then passed through a UF system to reduce silt density index (SDI) to less than 2. The characteristics of UF influent and permeate during a one-year period are summarized in Table 1. It is noted that the total Fe and Mn concentrations of the UF influent ranged from 0.18 to 4.52 mg/L of Fe and <0.1–0.25 mg/L of Mn. The presence of Mn was due to the addition of manganese alloys in basic-oxygen-furnace refinement process.

The UF system comprises three trains with total of 15 cassettes of submerged hollow fiber membranes (SUEZ Water). The UF membranes consist of polyvinylidene

fluoride (PVDF) with a nominal pore size of 0.04  $\mu\text{m}$ . The UF system was operated at a constant flux of 32 L/m<sup>2</sup>hr (LMH). The UF permeate was then polished with the RO unit to remove majority of dissolved salts and organics at a recovery rate of 65%. An ion exchange system was the final procedure to eliminate dissolved ions from the water by replacing them with H<sup>+</sup> and OH<sup>-</sup> ions to produce demineralized water. The IWPP has a designed capacity of 28,400 m<sup>3</sup>/day and can generate 4500 m<sup>3</sup>/day of RO permeate and 9000 m<sup>3</sup>/day of demineralized water.

Membrane maintenance cleaning was carried out once a week applying 100 mg/L sodium hypochlorite (NaOCl) and 2000 mg/L citric acid. When the UF trans-membrane pressure (TMP) exceeded – 45 kPa, recovery cleaning was implemented using 300 mg/L NaOCl and 2000 mg/L citric acid to recover membrane performance.

### Experimental timeline and analyses

The UF system in the IWPP demonstrated severe fouling problems after 3 years of operation. At this time, we began our investigation to identify the foulants by collecting samples of the UF membrane at 4 time points.

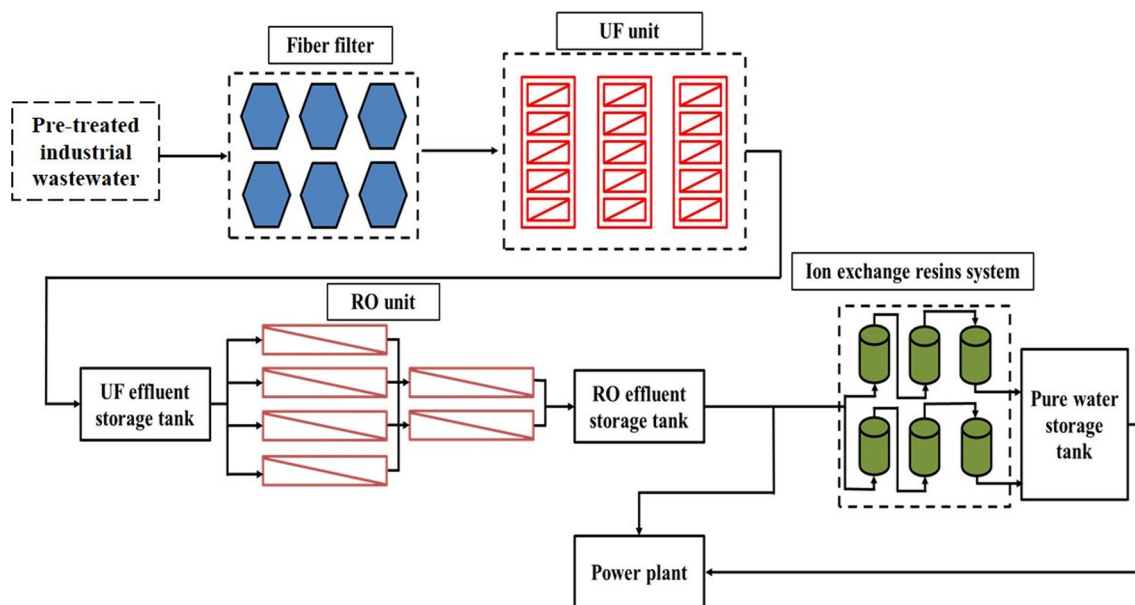


**Fig. 1** Schematic diagram of the IWPP in the integrated steelworks

**Table 1** Characteristics of UF influent and permeate during a one-year period

UF influent					UF permeate			
Turbidity (NTU)	pH	Conductivity ( $\mu\text{S}/\text{cm}$ )	COD (mg/L)	Fe (mg/L)	Mn (mg/L)	Turbidity (NTU)	pH	Conductivity ( $\mu\text{S}/\text{cm}$ )
5.26 $\pm$ 3.0	7.9 $\pm$ 0.38	5161 $\pm$ 168	42 $\pm$ 7	0.18–4.52	<0.1–0.25	0.27 $\pm$ 0.25	8.2 $\pm$ 0.32	4287 $\pm$ 400



The collection time points and the relevant experiments are depicted in the timeline as shown in Fig. 2. The UF membranes were cut from the same membrane cassette that is near to the UF inlet four times, which were labeled as A, B, C, and D in Fig. 2. Several experiments were conducted and will be described in the following sections.

### ICP-OES analysis for membrane foulants

At time points A and C, membranes were cut from the UF cassette, and the UF appearances of the time are shown in Fig. 3, respectively. The change in membrane color at time point C when compared to time point A suggests severe fouling by iron oxide as shown in Fig. 3b. A 30-cm-long membrane (cut at the middle part of the membrane) from the UF cassette was submerged in a 15-mL tube with 1% citric acid for 12 h. The citric acids were then analyzed by an inductively coupled plasma-optical emission spectroscopy (ICP-OES, PerkinElmer, Germany) to evaluate metallic concentrations in the foulants.

### SEM/EDS analysis

A SEM equipped with EDS (XB 1540 Crossbeam, Carl Zeiss SMT AG, Germany) was used to visualize and determine the elemental components of the membrane foulants on the membranes. All the membrane samples were obtained from the middle part of the membrane and dried at 50°C overnight and then coated with a thin carbon film to increase the conductivity prior to SEM/EDS analysis. It is critical to investigate the chemical components and spatial distribution of foulants in the membrane pores since the foulants deposited in the pores are more difficult to remove than those precipitated on the membrane surface. Therefore, we specifically examined the cross sections of the membrane samples using SEM/EDS to characterize the foulant depositing in the membrane pores. The membrane sample was frozen in liquid nitrogen and then immediately clipped by a sharp scissor (Zhou et al. 2015).

### Loss-on-ignition (LOI) analysis

The organic and inorganic constituents of the foulants were determined by LOI analysis. LOI was conducted at

**Fig. 2** Schematic diagram of the experimental timeline

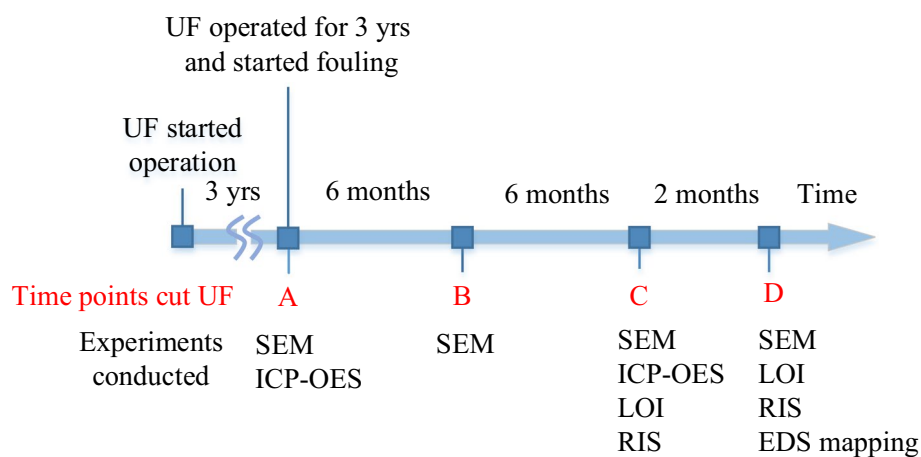


**Fig. 3** Pictures of the same UF cassette in the IWPP hung out to clean and examine membrane fouling at time point A and C, respectively. The dimension of the cassette is 2561 mm (height) × 2136 mm (width) × 1744 mm (depth)



time point C and D in duplicates. Membrane foulants were removed from a fouled UF membrane (1 m in length) by ultrasonic cleaning and then dried at 103 °C for 4 h to eliminate water. LOI can be obtained by calculating the weight of the sample before and after ignition at 550 °C. The LOI calculation was described in Eq. (1).

$$\text{LOI} = \frac{\text{weight(dry)} - \text{weight}(550^\circ\text{C})}{\text{weight(dry)}} \quad (1)$$

### Resistance-in-series (RIS) model

Resistance-in-series (RIS) model according to Darcy's law, as described in Eqs. (2) and (3), was applied to determine the components with changes in resistance that resulted from membrane fouling.

$$J = \frac{\Delta P}{\mu \cdot R_{\text{tot}}} \quad (2)$$

$$R_{\text{tot}} = R_m + R_{\text{re}} + R_{\text{irr}} + R_{\text{irc}} \quad (3)$$

$J$  is the membrane permeate flux ( $\text{m}^3/\text{m}^2/\text{sec}$ ),  $\Delta P$  is the trans-membrane pressure (TMP, Pa),  $\mu$  is the dynamic viscosity of the permeate (i.e., 0.001 Pa·s),  $R_{\text{tot}}$  is the total resistance ( $\text{m}^{-1}$ ) that can be quantified as the sum of the intrinsic membrane resistance ( $R_m$ ), the reversible fouling resistance ( $R_{\text{re}}$ ), the irreversible fouling resistance ( $R_{\text{irr}}$ ), and the irrecoverable fouling resistance ( $R_{\text{irc}}$ ). Reversible fouling can be eliminated by physical cleaning; irreversible fouling can only be removed by chemical cleaning; irrecoverable fouling cannot be mitigated by physical or

chemical cleaning (Park et al. 2015). A single-membrane reactor (Fig. 4) was applied to determine four types of resistances for the fouled membranes sampled at time point C and D. The test module with a 30-cm-long membrane cut at the middle part of the membrane was operated at a constant flux of  $4.15 \times 10^{-6} \text{ m}^3/\text{m}^2/\text{sec}$  for 30 min. The TMP value used to calculate the resistance was obtained by averaging a 10-min interval centered at the 25th min (i.e., average values from 20 to 30 min) of each test since the TMP reached stable at approximately the 20th min. First, deionized (DI) water was filtered through a new UF membrane to calculate the intrinsic membrane resistance ( $R_m$ ). Next, to determine the total fouling resistance (i.e.,  $R_{\text{re}} + R_{\text{irr}} + R_{\text{irc}}$ ), DI water was filtered through the fouled UF membrane cut from the IWPP. The reversible fouling resistance ( $R_{\text{re}}$ ) was then measured after physical cleaning (including backwash, aeration, and membrane relaxation). Afterward, chemical cleaning (1000 mg/L NaOCl for 5 h and 2000 mg/L citric acid for 5 h) was carried out to determine the irreversible fouling resistance ( $R_{\text{irr}}$ ), which is consisted of irreversible organic resistance, defined as the resistance obtained after NaOCl cleaning; and irreversible inorganic resistance, defined as the resistance obtained after citric acid cleaning. Once  $R_{\text{re}}$  and  $R_{\text{irr}}$  were obtained,  $R_{\text{irc}}$  can be calculated by subtracting them in  $R_{\text{re}} + R_{\text{irr}} + R_{\text{irc}}$ .

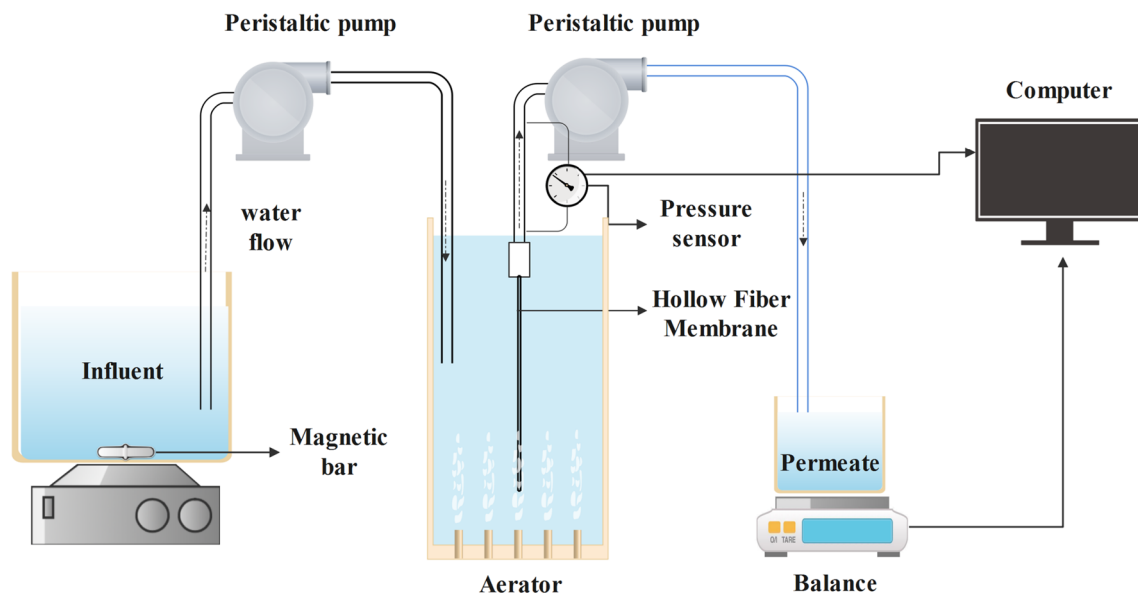


**Fig. 4** Schematic diagram of a single-membrane reactor

## Results and discussion

### Membrane foulants identification

#### ICP-OES results

To identify the metal constituents of the membrane foulants, the citric acid cleaners of UF membrane samples collected at time points A and C (as shown in Fig. 3) were analyzed using ICP-OES. The results demonstrated that Fe and Mn were the major metallic foulants (Table 2). Both the Fe and Mn concentrations at time point C are significantly higher than at time point A, particularly for the Mn concentration (19 mg/L in the citric acid). This finding further confirms that Fe in the UF influent caused the red-brown staining on the membrane surface as shown in Fig. 3b. We speculated that the foulants that caused the UF clogging could be iron and manganese oxides.

#### SEM/EDS analysis results

The surface topographies and cross-sectional images of the virgin and fouled membranes were visualized using SEM/EDS (Fig. 5). The elemental compositions of the red box areas scanned by SEM/EDS are presented in 3. Carbon and fluorine were primarily originated from PVDF materials. Figure 5a, b shows SEM surface and cross-sectional micrographs of a virgin membrane. Prior to foulant accumulation, the native surface and pores of PVDF membrane are smooth. Figure 5c–j shows the surface and cross-sectional micrographs of fouled membrane samples at four time points. At time point A (Fig. 5c), 5.73% of Fe, as the most abundant exogenous element, was found in the red box area, whereas Mn was not detected. The appearance of the membrane is shown in Fig. 3a. For the membrane sample at time point B, C, and D, respectively, condensed cake layers leading to TMP increase can be clearly observed on all membrane surface micrographs (Fig. 5e–i). Approximately 63.46%, 9.54%, and 8.73% of Fe and 1.4%, 31.29%, and 0.8% of Mn were found in the red box areas in Fig. 5e–i, respectively. The

**Table 2** ICP-OES results of the metallic concentrations in the citric acids (unit: mg/L)

Element	The membrane cut at time point A	The membrane cut at time point C
Ca	6.8	2.7
Mg	0.3	0.3
Fe	1.7	4.9
Mn	1.3	19
Si	0.2	0.4

abundance of Mn and Fe found by SEM/EDS corroborates with the high Mn and Fe concentrations detected in the citric acid by ICP-OES (Table 3). The SEM results suggested that iron and manganese oxides are the main foulants in the cake layer. In addition, the SEM micrographs and associated EDS analyses of the membrane cross section demonstrated that the foulants had formed within the membrane pores. The membrane structure includes an active and subjacent supporting layers. The active layer, where solid–liquid separation takes place during filtration, is the primary site of foulants accumulation. Fe and Mn were all detected in the UF active layers collected at the four time points as shown in Fig. 5d–j. Particularly, 14.42% of Mn is found in Fig. 5h, and 32.98% and 31.54% of Fe are found in Fig. 5d, j, respectively. The results obtained indicated that Mn and Fe ions can form metallic oxides within the membrane pores and could result in irreversible or irrecoverable fouling.

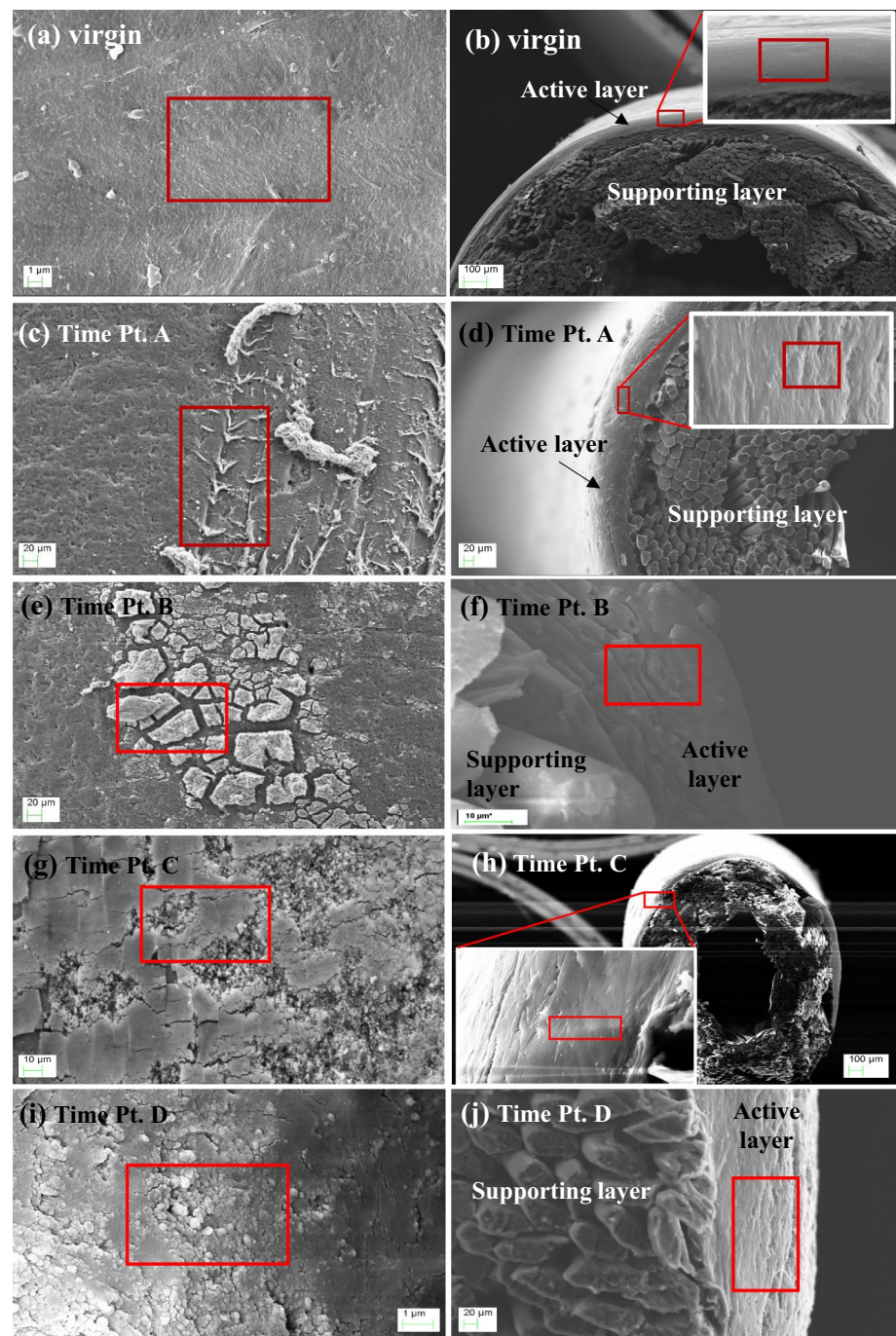
#### LOI results

LOI tests were carried out on membrane samples from time point C and D to determine the relative percentage of organic and inorganic compositions. The LOI result (Fig. 6) indicates that inorganic matters accounted for 53 ~ 55% of the foulants. Together with the ICP-OES and SEM/EDS findings, the iron and manganese oxides are likely to be the major constituents of the inorganic components of the foulants.

#### Determination of fouling resistance

Figure 7 presents the percentages of different fouling resistances in the fouled UF membrane samples at time point C and D. The intrinsic membrane resistance of the two virgin membranes accounted for only 3.21 and 1.38%. The reversible fouling resistance accounting for approximately 10 ~ 11% can be readily recovered by physical cleaning (backwash, aeration, and membrane relaxation in this study). Among the irreversible resistance, inorganic fouling resistance (determined after cleaning with citric acid) accounted for approximately 29%, while organic fouling resistance (determined after cleaning with NaOCl) accounted for only approximate 12%. The irrecoverable fouling resistance was expected to be the dominant contributor after 3 years of operation and accounted for 46.45 and 43.5% for the fouled UF samples at time point C and D, respectively. This result indicates that the inorganic matters with iron and manganese oxides as the major constituents, are the primary foulants that account for nearly 50% reduction in the functional capacity of the membrane.

**Fig. 5** SEM micrographs of the virgin and fouled membranes: **a** virgin membrane surface (10,000 $\times$ ); **b** virgin membrane cross section (700 $\times$ ); **c** fouled membrane surface cut at time point A (500 $\times$ ); **d** fouled membrane cross section cut at time point A (3000 $\times$ ); **e** fouled membrane surface cut at time point B (500 $\times$ ); **f** fouled membrane cross section cut at time point B (1200 $\times$ ); **g** fouled membrane surface cut at time point C (500 $\times$ ); **h** fouled membrane cross section cut at time point C (2000 $\times$ ); **i** fouled membrane surface cut at time point D (8000 $\times$ ); **j** fouled membrane cross section cut at time point D (3000 $\times$ ). EDS was used to scan the red box areas



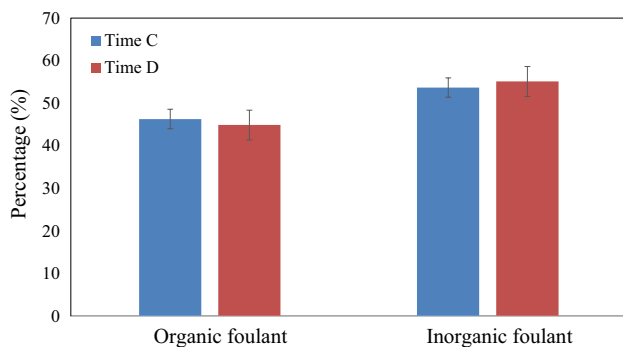
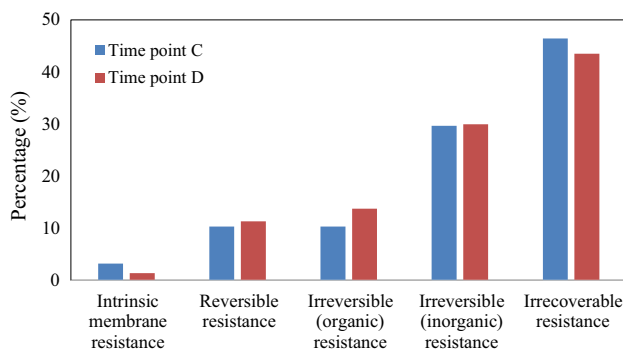
### Analysis of irrecoverable fouling

In this study, NaOCl (1000 mg/L) and citric acid (2000 mg/L) were applied sequentially to clean the fouled membrane by soaking and backwashing. The same fouled UF membrane, as previously seen in Fig. 5i, j, underwent chemical cleaning and was visualized by SEM as shown in Fig. 8a. In comparison with Fig. 5c, e, g, i, the fouling layer on the membrane surface was removed by chemical cleaning. Membrane pores are visualized in Fig. 8a, which

demonstrates that NaOCl and citric acid were sufficient to clean most foulants on the membrane surface. Figure 8b illustrates the SEM cross-sectional micrograph of the fouled membrane after chemical cleaning. The pores within the membrane cannot be visualized owing to the limited SEM resolution. The EDS analysis of the red box areas on the micrographs is listed in Table 4. Compared with Table 3, most of heavy metals on the surface were removed. However, Fe was still dominant in the red box area of the cross-sectional micrograph accounting for approximately 49% of

**Table 3** Elemental analysis of the red box areas on the SEM micrographs shown in Fig. 5 determined by EDS (unit: %)

Element	Virgin surface	Virgin cross section	A surface	A cross section	B surface	B cross section	C surface	C cross section	D surface	D cross section
C	59.03	–	70.77	–	14.7	49.18	22.45	–	38.62	–
O	–	14.64	2.48	2.43	11.07	2.61	10.53	68.75	26.24	35.99
F	38.02	84.44	17.95	5.71	–	38.96	23.39	5.34	19.95	2.96
Mg	–	–	–	–	–	–	0.12	–	0.27	1.83
Al	–	–	0.44	0.14	0.62	–	0.27	0.57	1.46	3.84
Si	–	0.91	1.23	0.72	1.46	0.66	–	0.62	–	2.83
P	–	–	–	–	2.15	–	–	–	–	–
S	–	–	–	1.17	–	–	–	0.61	–	1.96
Zn	–	–	–	0.32	0.75	–	–	0.47	0.17	0.45
Cl	0.26	–	0.47	7.84	1.00	–	0.98	1.36	1.42	3.64
Ca	–	–	0.41	39.44	1.37	–	1.42	1.48	2.34	11.27
Cr	–	–	–	4.57	–	–	–	–	–	–
Mn	–	–	–	4.68	1.4	5.12	31.29	14.42	0.80	1.81
Fe	–	–	5.73	32.98	63.46	3.48	9.54	5.63	8.73	31.54
Cu	–	–	–	–	0.06	–	–	–	–	–
Ag	–	–	0.18	–	–	–	–	–	–	–
Au	2.69	–	0.33	–	1.94	–	–	–	–	–

**Fig. 6** LOI measurement of membrane foulants**Fig. 7** Percentages of different resistances in the fouled UF membrane

the total elements. This observation indicates that iron oxide accumulated within the membrane pores cannot be efficiently cleaned by chemical reagents. Mn was not detected on the membrane surface (Fig. 8a) but accounted for approximately 1% within the membrane pores (the red box area in Fig. 8b). We can also infer that chemical cleaning was not efficient at removing manganese oxide from the pores. To sum up, iron and manganese oxides were responsible for the irrecoverable fouling in the fouled membranes since foulants in the membrane pores were considered to be irrecoverable (Jiang et al. 2003).

The EDS mapping of the cross section of the fouled membrane was conducted after chemical cleaning to verify the impact of Fe and Mn on membrane fouling. Figure 9 shows a cross-sectional micrograph and EDS mapping images of the fouled UF membrane after chemical cleaning. In Fig. 9b, c, iron and manganese oxides were uniformly scattered in the active and supporting layers. In the IWPP, most Fe ions in the feed solution were readily oxidized to iron oxides since the UF system was aerated at neutral pH to prevent membrane fouling (Choo et al. 2005). However, the remaining non-oxidized Fe ions and small iron oxide particulates can still pass through the membrane surface. Formation of larger iron oxide particulates can occur in the membrane pores leading to irrecoverable fouling. In comparison with Fe ions, Mn ions do not oxidize as easily. In the IWPP, the addition of hypochlorous acid was carried out to mitigate biofouling prior to the fiber filtration. Chlorination facilitates oxidation





**Fig. 8** SEM micrographs of the fouled membrane after chemical cleaning: **a** surface (3000×); **b** cross section (1000×)

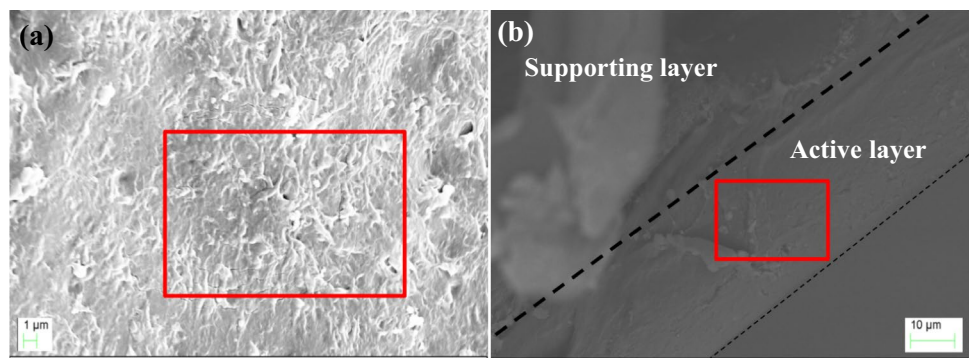


**Table 4** Elemental analysis of the red box areas on the SEM micrographs shown in Fig. 8

Element	Surface (%)	Cross section (%)
C	46.57	34.98
O	15.41	7.99
F	33.35	6.74
Ca	2.8	–
Fe	1.87	49.29
Mn	–	1.0

of Mn ions, which can accumulate as manganese particles in the membrane pores and then progressively make manganese oxide particles grow up in the membrane pores (Podaru et al. 2008). In summary, we demonstrate that irrecoverable UF membrane fouling begins with the oxidation of Fe and Mn ions and followed by the deposit of the oxide particulates in the membrane pores. Thus, based on our findings, removal of Fe and Mn in the pretreatment of the UF influent can be an effective way to mitigate irrecoverable fouling by Fe and Mn oxides in the IWPP.

**Fig. 9** **a** SEM cross-sectional micrograph and **b, c** the EDS mapping images of the fouled UF membrane after chemical cleaning

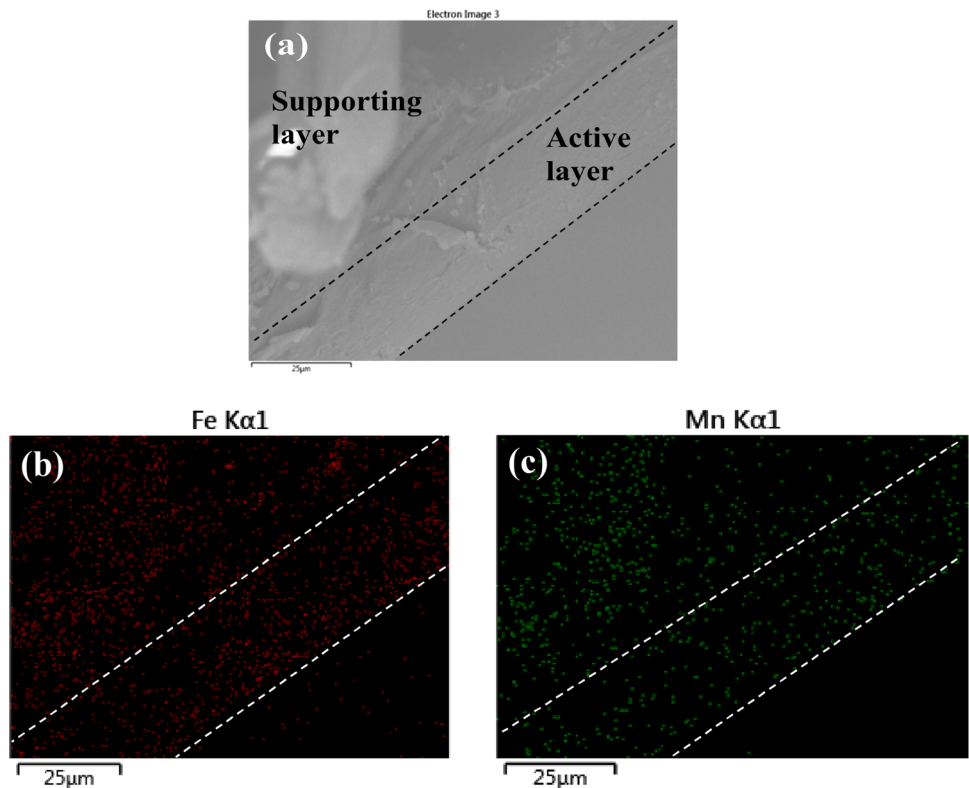


**Fig. 10** Schematic diagrams of two hypothesized mechanisms of membrane fouling caused by Fe and Mn oxide particulates

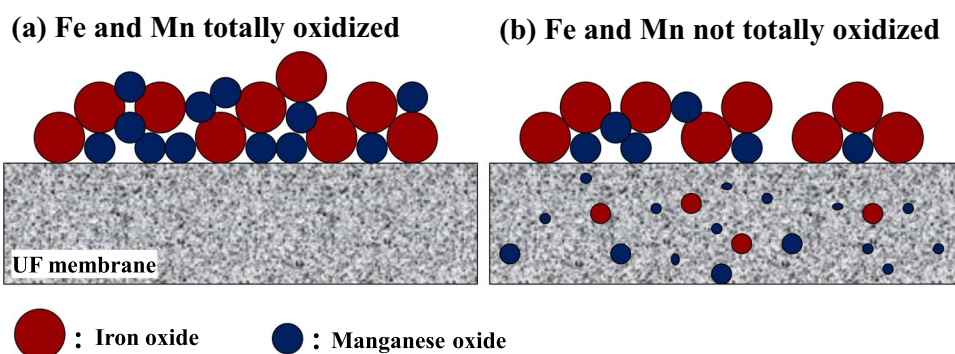


**Table 5** Standard electrode potentials for reduction half-reactions (Stumm and Morgan 1996)

Reduction reaction	Standard electrode potential, $E^0$ (V) at 25°C
$\text{MnO}_{2(s)} + 4\text{H}^+ + 2\text{e}^- = \text{Mn}^{2+} + \text{H}_2\text{O}$	1.23
$\text{Fe}^{3+} + \text{e}^- = \text{Fe}^{2+}$	0.77
$\alpha\text{-FeOOH}_{(s)}^* + 3\text{H}^+ + \text{e}^- = \text{Fe}^{2+} + 2\text{H}_2\text{O}$	0.67
$1/2\alpha\text{-Fe}_2\text{O}_{3(s)}^\# + 3\text{H}^+ + \text{e}^- = \text{Fe}^{2+} + 3/2\text{H}_2\text{O}$	0.66

\* $\alpha\text{-FeOOH}$ : goethite;  $\# \alpha\text{-Fe}_2\text{O}_3$ : hematite

## Membrane fouling mechanisms

The experimental results and observations presented in this paper show that the formation of Fe and Mn oxide particulates represents a major mechanism of severe membrane fouling in the UF system in the IWPP. Figure 10 illustrates two possible mechanisms of the fouling phenomenon caused by iron and manganese oxide particulates. If the Fe and Mn ions are totally oxidized in the influent, the cake layer formed by the metallic oxides on the membrane surface might not cause serious fouling but rather can ameliorate permeability (Fig. 10a) since the oxide particles can adsorb organic matters, which can act as foulants (Chang et al. 1998; Lee et al. 2002). Although addition of hypochlorous acid in the UF influent and aeration in the UF trains oxidizes Fe and Mn ions, part of the Fe and Mn ions and oxide particulates are still tiny enough to deposit within the pores after chlorination, ultimately leading to clogging of the pores (Fig. 10b). In addition, the slow oxidation rate of Mn (Choo Lee and Choi 2005) increases the likelihood for Mn oxides to deposit and accumulate within the pores. Manganese oxide, particularly manganese dioxide, can catalyze Mn and Fe oxidation (i.e., autocatalytic process) (Chen et al. 2011; Cheng et al. 2020; Teng et al. 2001), which will continue to adsorb and catalyze the Mn and Fe ions that enter the pores, and oxidize both ions to oxide forms, causing pore blocking and irrecoverable fouling. The reduction potentials of  $\text{MnO}_2/$

$\text{Mn}^{2+}$  and Fe ions/Fe oxides are listed in Table 5 as well to support this statement.

## Conclusion

The fouled UF membranes after 3 years of operation in the IWPP were conducted a series of analysis to identify the main foulants that severely clogged the UF membranes. Our investigations identify Fe and Mn as the main heavy metal foulants on the membranes. Based on SEM/EDS results, the fouling layer on the membrane surface mainly contained Fe (highest 63.46%) and Mn (highest 31.29%). Within the cross section of the fouled UF membranes, high percentages of Fe (highest 32.98%) and Mn (highest 14.42%) were found in the active layers. We further demonstrate that oxidation of Fe and Mn can occur as deposits on the membrane surface and within the membrane pores and is the major mechanism in the formation of irreversible or irrecoverable fouling. In addition, the LOI analysis showed that inorganic foulants accounted for 53 ~ 55%, further supporting the role of iron and manganese oxides as the major foulants. Resistance-in-series model analysis showed that the irrecoverable resistance accounted for approximately 43 ~ 47% of the total resistance, whereas the irreversible resistance, including inorganic resistance (29.68%) and organic resistance (10.34%), accounted for approximately 40%. After the fouled membrane underwent chemical cleaning, residual Fe and Mn compounds were identified in the membrane pores by SEM/EDS and EDS mapping. The results demonstrated that the irrecoverable fouling can be attributed to the deposit of Fe and Mn ions and oxide particulates in the membrane pores, and the subsequent autocatalytic oxidation of Fe and Mn ions further accumulates oxide particulates that ultimately results in pore blocking and irrecoverable fouling. Therefore, based on our findings, removal of Fe and Mn ions can be a sound strategy to mitigate irrecoverable fouling resulted in the IWPP.



**Acknowledgements** This study was supported by the National Science and Technology Council, Taiwan (Grant No. MOST 107-2218-E-008-021-MY2). The authors would like to thank the Precision Instrument Support Center of National Central University in providing the analysis facilities.

**Author' contributions** P-HL contributed to the experimental design, interpretation of results, and manuscript preparation; Y-CS conducted laboratory analysis, designed the experiments, and interpretation; C-LC contributed to data analysis, interpretation of results, and revision of the manuscript. I-YT conducted laboratory analysis and interpretation of results. All authors read and approved the final manuscript.

## Declarations

**Conflict of interest** The authors declare they have no competing interests.

**Ethical approval** This article does not contain any studies with human participants or animals performed by any of the authors.

## References

- Al Aani S, Wright CJ, Hilal N (2018) Investigation of uf membranes fouling and potentials as pre-treatment step in desalination and surface water applications. *Desalination* 432:115–127. <https://doi.org/10.1016/j.desal.2018.01.017>
- Baker RW (2004) *Membrane technology and applications*, 2nd edn. Wiley, Chichester
- Bourgeois KN, Darby JL, Tchobanoglous G (2001) Ultrafiltration of wastewater: effects of particles, mode of operation, and backwash effectiveness. *Water Res* 35(1):77–90. [https://doi.org/10.1016/S0043-1354\(00\)00225-6](https://doi.org/10.1016/S0043-1354(00)00225-6)
- Chang YJ, Choo KH, Benjamin MM, Reiber S (1998) Combined adsorption-uf process increases toc removal. *J Am Water Works Assoc* 90(5):90–102. <https://doi.org/10.1002/j.1551-8833.1998.tb08438.x>
- Chen W-H, Hsieh Y-H, Wu C-C, Wan M-W, Futralan CM, Kan C-C (2011) The on-site feasibility study of iron and manganese removal from groundwater by hollow-fiber microfiltration. *J Water Supply Res Technol AQUA* 60(6):391–401. <https://doi.org/10.2166/aqua.2011.067>
- Cheng L-H, Xiong Z-Z, Cai S, Li D-W, Xu X-H (2020) Aeration-manganese sand filter-ultrafiltration to remove iron and manganese from water: oxidation effect and fouling behavior of manganese sand coated film. *J Water Process Eng* 38:101621. <https://doi.org/10.1016/j.jwpe.2020.101621>
- Choi SK, Haakrho Y, Moon J, Sung Y, Kang SG (2015) Fouling characteristics of uf and ro membranes for reclamation of the wastewater from iron and steel industry. *Int J Environ Sci* 5(4):709–716. <https://doi.org/10.6088/ijes.2014050100066>
- Choo KH, Lee H, Choi SJ (2005) Iron and manganese removal and membrane fouling during uf in conjunction with prechlorination for drinking water treatment. *J Membr Sci* 267(1):18–26. <https://doi.org/10.1016/j.memsci.2005.05.021>
- Colla V, Branca TA, Rosito F, Lucca C, Vivas BP, Delmiro VM (2016) Sustainable reverse osmosis application for wastewater treatment in the steel industry. *J Clean Prod* 130:103–115. <https://doi.org/10.1016/j.jclepro.2015.09.025>
- Darton T, Annunziata U, del Vigo Pisano F, Gallego S (2004) Membrane autopsy helps to provide solutions to operational problems. *Desalination* 167:239–245. <https://doi.org/10.1016/j.desal.2004.06.133>
- D'Souza NM, Mawson AJ (2005) Membrane cleaning in the dairy industry: a review. *Crit Rev Food Sci Nutr* 45(2):125–134. <https://doi.org/10.1080/10408690490911783>
- Field RW, Wu JJ (2011) Modelling of permeability loss in membrane filtration: re-examination of fundamental fouling equations and their link to critical flux. *Desalination* 283:68–74. <https://doi.org/10.1016/j.desal.2011.04.035>
- Gao W, Liang H, Ma J, Han M, Chen ZL, Han ZS, Li GB (2011) Membrane fouling control in ultrafiltration technology for drinking water production: a review. *Desalination* 272(1–3):1–8. <https://doi.org/10.1016/j.desal.2011.01.051>
- Guo W, Ngo HH, Li J (2012) A mini-review on membrane fouling. *Bioresour Technol* 122:27–34. <https://doi.org/10.1016/j.biortech.2012.04.089>
- Hird W (2006) Recycled water—case study: bluescope steel, port kembla steelworks. *Desalination* 188(1):97–103. <https://doi.org/10.1016/j.desal.2005.04.106>
- Huang XF, Ling J, Xu JC, Feng Y, Li GM (2011) Advanced treatment of wastewater from an iron and steel enterprise by a constructed wetland/ultrafiltration/reverse osmosis process. *Desalination* 269(1):41–49. <https://doi.org/10.1016/j.desal.2010.10.040>
- Jafari M, Vanoppen M, van Agtmaal JMC, Cornelissen ER, Vrouwenvelde JS, Verliefde A, van Loosdrecht MCM, Picioreanu C (2021) Cost of fouling in full-scale reverse osmosis and nanofiltration installations in the Netherlands. *Desalination* 500:114865. <https://doi.org/10.1016/j.desal.2020.114865>
- Jiang T, Kennedy MD, van der Meer WGG, Vanrolleghem PA, Schippers JC (2003) The role of blocking and cake filtration in mbr fouling. *Desalination* 157(1):335–343. [https://doi.org/10.1016/S0011-9164\(03\)00414-4](https://doi.org/10.1016/S0011-9164(03)00414-4)
- Katsoufidou KS, Sioutopoulos DC, Yiantsios SG, Karabelas AJ (2010) Uf membrane fouling by mixtures of humic acids and sodium alginate: fouling mechanisms and reversibility. *Desalination* 264(3):220–227. <https://doi.org/10.1016/j.desal.2010.08.017>
- Lee KW, Choo KH, Choi SJ, Yamamoto K (2002) Development of an integrated iron oxide adsorption/membrane separation system for water treatment. *Water Supply* 2(5–6):293–300. <https://doi.org/10.2166/ws.2002.0182>
- Lee JW, Kwon TO, Moon IS (2005) Performance of polyamide reverse osmosis membranes for steel wastewater reuse. *Desalination* 177(1):69–82. <https://doi.org/10.1016/j.desal.2004.10.033>
- Michael-Kordatou CM, Duan X, He X, Dionysiou DD, Mills MA, Fatta-Kassinos D (2015) Dissolved effluent organic matter: characteristics and potential implications in wastewater treatment and reuse applications. *Water Res* 77:213–248
- Mohammadi T, Esmaeilifar A (2004) Wastewater treatment using ultrafiltration at a vegetable oil factory. *Desalination* 166:329–337. <https://doi.org/10.1016/j.desal.2004.06.087>
- Nguyen ST, Roddick RF (2011) Chemical cleaning of ultrafiltration membrane fouled by an activated sludge effluent. *Desalin Water Treat* 34:94–99
- Park H-D, Chang I-S, Lee K-J (2015) *Principles of membrane bioreactors for wastewater treatment*. CRC Press, Boca Raton
- Petricic I, Korenak J, Povodnik D, Hélix-Nielsen C (2015) A feasibility study of ultrafiltration/reverse osmosis (uf/ro)-based wastewater treatment and reuse in the metal finishing industry. *J Clean Prod* 101:292–300. <https://doi.org/10.1016/j.jclepro.2015.04.022>
- Podaru C, Danielescu C, Sonea D, Pacala A, Vlaicu I, Cosma C, Burtica G, Manea F, Orha C (2008) A comparative study of two groundwater treatment pilot plants. *Water Pollut IX* 111:149–157. <https://doi.org/10.2495/wp080151>
- Porcelli N, Judd S (2010) Chemical cleaning of potable water membranes: the cost benefit of optimisation. *Water Res* 44(5):1389–1398. <https://doi.org/10.1016/j.watres.2009.11.020>
- Racar M, Dolar D, Špehar A, Košutić K (2017) Application of uf/nf/ro membranes for treatment and reuse of rendering plant wastewater.



- Process Saf Environ Prot 105:386–392. <https://doi.org/10.1016/j.psep.2016.11.015>
- Rohani R, Hyland M, Patterson D (2011) A refined one-filtration method for aqueous based nanofiltration and ultrafiltration membrane molecular weight cut-off determination using polyethylene glycols. *J Membr Sci* 382(1–2):278–290. <https://doi.org/10.1016/j.memsci.2011.08.023>
- Shi X, Tal G, Hankins NP, Gitis V (2014) Fouling and cleaning of ultrafiltration membranes: a review. *J Water Process Eng* 1:121–138. <https://doi.org/10.1016/j.jwpe.2014.04.003>
- Stumm W, Morgan JJ (1996) *Aquatic chemistry, chemical equilibria and rates in natural waters*, 3rd edn. Wiley, New York
- Teng Z, Yuan Huang J, Fujita K, Takizawa S (2001) Manganese removal by hollow fiber micro-filter membrane separation for drinking water. *Desalination* 139(1):411–418. [https://doi.org/10.1016/S0011-9164\(01\)00342-3](https://doi.org/10.1016/S0011-9164(01)00342-3)
- Zhou FL, Parker GJM, Eichhorn SJ, Hubbard Cristinacce PL (2015) Production and cross-sectional characterization of aligned co-electrospun hollow microfibrous bulk assemblies. *Mater Charact* 109:25–35. <https://doi.org/10.1016/j.matchar.2015.09.010>

Springer Nature or its licensor (e.g. a society or other partner) holds exclusive rights to this article under a publishing agreement with the author(s) or other rightsholder(s); author self-archiving of the accepted manuscript version of this article is solely governed by the terms of such publishing agreement and applicable law.

